Phase retrieval from double axially displaced holograms for dual-wavelength in-line holography

Yan Li (李 艳)[1*], Wen Xiao (肖 文)[1], Feng Pan (潘 锋)[1], and Lu Rong (戎 路)[2]

[1]*Key Laboratory of Precision Opto-mechatronics Technology, Ministry of Education, Beihang University, Beijing 100191, China*

[2]*College of Applied Sciences, Beijing University of Technology, Beijing 100124, China*

[*]*Corresponding author: lyx0514@aspe.buaa.edu.cn*

Received September 25, 2013; accepted December 12, 2013; posted online January 27, 2014

A phase retrieval method for dual-wavelength in-line digital holography is presented with double axially displaced holograms. A synthetic wavelength is used during iterative propagations to retrieve wrap-free phase distributions with a much extended measurement range. The simulation and experimental results demonstrate a better elimination of the twin image, a faster rate of convergence of the iterative routine and less number of wavelengths are compared with previously reported multiple-wavelength in-line holography.

OCIS codes: 090.1995, 100.5070, 100.3010.

doi: 10.3788/COL201412.020901.

In-line holography[1], owing to no optical elements before the detector, is a suitable imaging tool in visible spectrum[2], short-wavelength spectrum[3,4], and particle-field analysis[5]. However, the hologram is formed by the interference between the free propagated light as the reference beam and the diffracted object wave, both of which propagate along the same direction downstream the light source. Therefore, the defocused image and zero-order term are superimposed onto the real image in the reconstruction process[2−5], which deteriorates the image quality and degrades the measurement accuracy.

Various methods have been proposed to eliminate or minimize this inherent limitation in in-line holography. Early methods, including superposition of holograms from multiple wavelengths[6,7] and hologram subtraction at different recording planes[8,9], are only suitable for electron digital holographic microscopy or X-ray digital holographic microscopy. Digital techniques, such as linear filtering[10], only suppress rather than eliminate the twin image. Phase retrieval algorithms provide an effective solution for twin image elimination. By involving the iterative diffraction propagations back and forth between the object and the recording domains, real image is well separated from the unwanted conjugate image. For some iterative algorithms use square module constraint on the recording plane without imposing any constraint on the object plane[11,12], the convergence of which is very likely to be trapped into local minimum[13]. In other algorithms, the amplitude of single hologram is imposed on the recording plane as the constraint, of which the convergence is guaranteed via other constraints on the object plane[14−16]. We developed a phase retrieval method using two axially displaced holograms combined with a finite transmission constraint on the object plane to eliminate the conjugate image, and it has been demonstrated that this approach has much faster speed of convergence and better elimination effect[17]. The methods above only allow for the determination of the phase modulo 2π, and in some cases this is not sufficient. For objects, whose optical thickness variations are greater than the wavelength, the phase images are wrapped in the range of $(-\pi, \pi]$ radians after actangent calculation[18]. Bao *et al.* presented phase retrieval technique based on multiple wavelengths to extend the range of measurement[19,20]. Since there is no object constraint, it requires a large number of illumination wavelengths and the convergence is not guaranteed.

In this letter, a phase retrieval method for dual-wavelength in-line digital holography has been proposed for dispersion-free objects, in which iteration calculation is performed using double axially displaced holograms recorded at dual-wavelengths respectively. A synthetic wavelength is used to calculate the wrap-free phase, as in two-wavelength interferometry[18]. The appropriate constraints are imposed both on the hologram plane and object plane, thus faster speed of convergence and better elimination effect are realized with less number of wavelengths compared with those of previous reported approaches in Refs. [19,20]. Meanwhile, more accurate unambiguous unwrapped phase distributions are achieved because of synthetic wavelength. The feasibility of this method is validated by the numerical simulations and related experiments.

The schematic diagram of the setup is illustrated in Fig. 1. The beam derived from a tunable laser was expanded and collimated by a beam expander (composed of a spatial filter and a collimating lens), then passed though the sample. A complementary metal-oxide-semiconductor (CMOS) located consequtively at the distance z_1 and z_2 downstream of the sample was utilized to record four holograms at both dual wavelengths of 643.0 and 658.0 nm, which determined that the corresponding synthetic wavelength Λ used in iteration was 28.2 μm. The background images were taken in the same condition in the absence of the object. The corresponding normalized holograms were carried out by dividing the holograms by background images in every hologram planes[15,16].

The main iterative procedures are as follows.

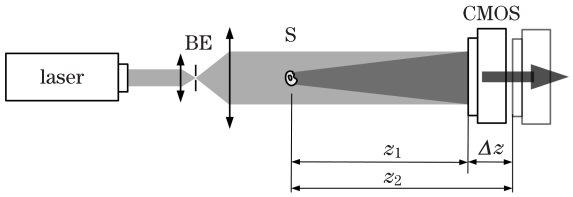

Fig. 1. Schematic diagram of the setup. BE: beam expander with spatial filter; S: sample; z_1: the first recording distance (reconstruction distance); z_2: the second recording distance (reconstruction distance); Δz: distance interval.

1) Two iterative calculations start respectively with initial guessed phases $\phi_{\lambda_n}(x_1, y_1)\,(n = 1, 2)$, where (x_1, y_1) are the coordinate in the first hologram plane with shorter recording distance z_1. $\exp(j\phi_{\lambda_n}(x_1, y_1))$ are multiplited with the square roots of the corresponding normalized holograms to yield the complex amplitude distributions $U_{\lambda_n}(x_1, y_1)$ at the first hologram planes:

$$U_{\lambda_n}(x_1, y_1) = \sqrt{H_{\lambda_n}(x_1, y_1)/G_{\lambda_n}(x_1, y_1)} \cdot \exp\left[j\phi_{\lambda_n}(x_1, y_1)\right]. \quad (1)$$

2) $U_{\lambda_n}(x_1, y_1)$ propagates back to the corresponding object planes with the distance z_1 by the angular spectrum propagation (ASP) integral[21], which is valid for short-distance propagations and keeps the same image size when the reconstruction distance changes.

$$\begin{aligned} U_{\lambda_n}(x_o, y_o) &= ASP_{-z_1}\left[U_{\lambda_n}(x_1, y_1)\right] \\ &= A_{\lambda_n}(x_o, y_o)\exp\left[j\phi_{\lambda_n}(x_o, y_o)\right], \end{aligned} \quad (2)$$

where (x_o, y_o) is the coordinate in the object plane, $A_{\lambda_n}(x_o, y_o)$ and $\phi_{\lambda_n}(x_o, y_o)$ are the amplitude and phase distributions of $U_{\lambda_n}(x_o, y_o)$ in the object plane.

3) The complex amplitude distributions in the object plane should satisfy with two constraints. Due to the positive absorption of the object, the amplitude of the transmission function in the object plane should not exceed one[17]. The interference between the twin image and the unscattered wave results in those emerging negative absorptions, therefore the amplitudes of those regions are replaced as

$$U'_{\lambda_n}(x_o, y_o) = \begin{cases} U_{\lambda_n}(x_o, y_o) & A_{\lambda_n}(x_o, y_o) \leqslant 1 \\ 1 & \text{otherwise} \end{cases}. \quad (3)$$

4) $U'_{\lambda_n}(x_o, y_o)$ propagate forward to the second recording planes at longer recording distance z_2 and form the complex amplitude $U_{\lambda_n}(x_2, y_2)$, where (x_2, y_2) is the coordinate in the second hologram plane. The amplitudes are replaced by the square roots of the normalized holograms at this plane, and the phase distributions are extracted.

$$U_{\lambda_n}(x_2, y_2) = \sqrt{H_{\lambda_n}(x_2, y_2)/G_{\lambda_n}(x_2, y_2)} \cdot \exp\left[j\phi_{\lambda_n}(x_2, y_2)\right]. \quad (4)$$

5) The updated complex amplitudes propagate back to the object planes, and the new complex amplitudes $U''_{\lambda_n}(x_o, y_o)$ are modulated using the same object constraints in step 2. Calculating the synthetic phase from the two phases:

$$\phi''_{\lambda_\Lambda}(x_o, y_o) = \begin{cases} \phi''_{\lambda_1}(x_o, y_o) - \phi''_{\lambda_2}(x_o, y_o) & \phi''_{\lambda_1}(x_o, y_o) > \phi''_{\lambda_2}(x_o, y_o) \\ \phi''_{\lambda_1}(x_o, y_o) - \phi''_{\lambda_2}(x_o, y_o) + 2\pi & \text{otherwise} \end{cases}, \quad (5)$$

where $\phi''_{\lambda_n}(x_o, y_o)$ are the phases of $U''_{\lambda_n}(x_o, y_o)$, and λ_Λ is the synthetic wavelength[18]:

$$\lambda_\Lambda = \lambda_1\lambda_2/\left(\lambda_2 - \lambda_1\right). \quad (6)$$

The object surface height profile $h(x_o, y_o)$ can be calculated according to[20]

$$h(x_o, y_o) = \lambda_\Lambda \cdot \phi''_{\lambda_\Lambda}(x_o, y_o)/2\pi n_\Delta, \quad (7)$$

where $n_\Delta = n - n_0$ is the refractive index difference between the sample and the surrounding medium.

Thus, the wavelength interval should be arranged to guarantee that the synthetic wavelength optical path length exceeds the maximum height variation of the object surface to avoid phase unwrapping. $\phi''_{\lambda_n}(x_o, y_o)$ are converted by the unambiguous unwrapped phase distributions according to the object surface height profile $h(x_o, y_o)$, while the amplitudes are reserved as

$$\phi_{\lambda_n}(x_o, y_o) = 2\pi(n - n_0) \cdot h(x_o, y_o)/\lambda_n. \quad (8)$$

6) Combining the amplitudes and phases at each illumination wavelength yields two wavefronts at each object plane:

$$U_{\lambda_n}(x_o, y_o) = \left|U''_{\lambda_n}(x_o, y_o)\right| \exp\left[j\phi_{\lambda_n}(x_o, y_o)\right], \quad (9)$$

then propagating forward to the first recording plane respectively. The amplitudes are replaced with the square root of the normalized holograms at these planes, while the phase distributions are extracted, and used as the input values for the next iteration starting at step 2. The complex amplitudes are updated and corrected during the iterations. Further iterations eventually lead to the elimination of twin image, and retrieve unambiguous unwrapped phase distributions.

To validate the feasibility of the proposed algorithm, we simulated the in-line hologram using a two-dimensional (2D) complex object as shown in Fig. 2(a). It is composed of four alphabetic characters with a constant absorption of 20% of the incident coherent beam and different height distributions of 5, 8, 12, and 20 μm. Suppose the refractive index of simulated object is 1.5, resulting in the phase shifts is 0.56, 0.89, 1.34, and 2.23 rad, respectively, for the synthetic wavelength Λ of 28.2 μm used in iteration, which was larger than the maximum height of the object. A camera with 1024×1024 pixels of size 6.7×6.7 (μm) was utilized for recording holograms. The holograms were numerically formed at distances of 140 and 142 mm away from the object, respectively, at every recording wavelengths of 643.0 and 658.0 nm, and the holograms with the distance of 140 mm at both wavelengths are displayed in Fig. 2(b). The method of the phase retrieval using double sequences intensity patters (PRDS)[20] was also used for comparison, and the reconstructed results after 100 iterations are shown in Fig. 2(c). The structures of the reconstructed images obtained from the method in Ref. [20] are distorted because of the twin-image contamination. The retrieved

images from the proposed method after the same iterations are shown in Fig. 2(d). The lines scan show that the twin image has been completely removed after iterative calculation, and the reconstructed field has reached its predefined value.

The convergence rate is the key indicator for iterative algorithms, which can be monitored in the iterations by the mean square error (MSE). It is defined as

$$\mathrm{MSE}^n = \frac{1}{M \times N} \sum_{\substack{\xi = 1,2,\cdots M \\ \eta = 1,2,\cdots N}} \left[\rho^n(\xi,\eta) - \rho_{\mathrm{o}}(\xi,\eta)\right]^2, \tag{10}$$

where $\rho^n(\xi,\eta)$ is the retrieved amplitude of the object transmission function or the retrieved height distribution, $\rho_{\mathrm{o}}(\xi,\eta)$ is the corresponding original one, and N, M denote the matrix sizes of the object domain. The noise influence was also investigated by simulation. The shot noise, which follows a Poisson's statistics[22], was added to the normalized hologram. The signal-to-noise ratio (SNR) of the noisy hologram is the reciprocal of the contrast, which is 14.3 dB[23]. The corresponding comparison of the convergence rates are shown in Fig. 3. The logarithmic scale of MSE is used on the y-axis label in order to express the conclusion more clearly. Comparing with the method in Ref. [20], the proposed approach has a faster rate of convergence and better elimination of the twin image after same number of iterations. Meanwhile, the proposed method provides a better tolerance of noise.

The influence of experimental parameters on convergence performance was evaluated. The pattern of "lena" was used in the simulation, the gray level of which indicates the height profile of a 2D complex object with the maximum height of 20 μm, as shown in Fig. 4(a). Figure 4(b) shows the lg(MSE) versus the number of iterations when the wavelength intervals $|\lambda_p - \lambda_q|$ are 2, 5, 10, 15, and 20 nm. It is noticed that the larger interval between the two wavelengths has a faster rate of convergence and better elimination effect after same number of iterations, while the curves with the wavelength intervals of 15 and 20 nm are at the same convergence and elimination effect. Since larger synthetic wavelength would amplify the noise, two wavelengths should be separated far enough to satisfy the maximum level of phase noise[18]. Figure 4(c) presents that the performance of proposed method are not related to the number of used illumination wavelengths when constraints are imposed on both the hologram planes and object plane. When the number of wavelengths was reduced from 31 to 2, the convergence speed is almost the same. On the other hand, the convergence of the algorithm in Ref. [20] required no less than 10 illumination wavelengths. The influence of axial sampling interval is shown in Fig. 4(d). The elimination effect is worse when the interval increases, while the rate of convergence is same.

Experiments were performed in order to verify the method (Fig. 1). A tunable diode laser (Xperay-TL STD, Nanobase Inc, Korea) with a wavelength tuning range between 640 and 675 nm was used as the light source. A binary phase grating with 1-μm etching depth and 300-μm period was used as the sample, and the refractive index of the sample was approximately 1.5. A CMOS (Lumenera, LU-125M) with 1280×1024 pixels of size 6.7×6.7 (μm) was utilized to record the hologram, but only 1024×1024 pixels were used to get efficient fast Fourier transform (FFT) calculation. Four holograms were recorded consequtively at the distances of 99- and 100-mm downstream of the sample at both wavelengths of 643.0 and 658.0 nm. The corresponding synthetic wavelength Λ was extended to 28.2 μm, and the exact distance was obtained via Laplacian second-order differentiation auto-focusing method[24]. The corresponding backgrounds were taken under the same condition in the absence of the object.

The holograms and the reconstruction results are shown in Fig. 5. Figure 5(a) shows two in-line holograms recorded at the wavelengths of 643.0 and 658.0 nm with distance of 99 mm. As seen in Fig. 5(b), the object distribution is still obscured by twin image after 100 iterations using method in Ref. [20]. It is clearly shown in Fig. 5(c) that after the same number of iterations the residual fringes are gone and height distributions are truthfully recovered by the proposed method. Figure

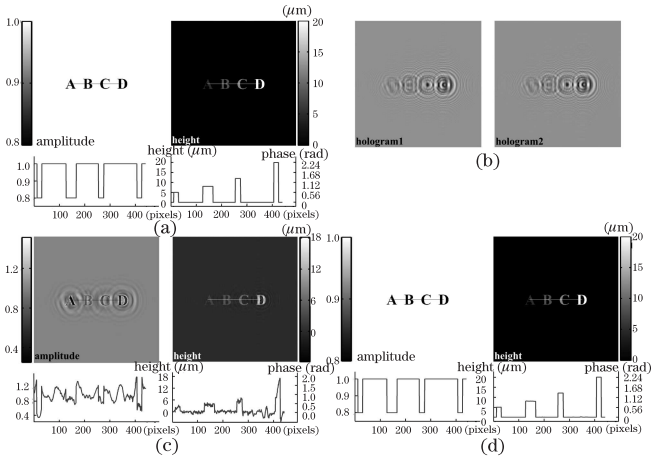

Fig. 2. Amplitude and phase reconstructions of a simulated 2D complex-valued object. (a) Original distribution in the object plane; (b) simulated hologram using conventional integral with wavelengths of 643.0 and 658.0 nm respectively; (c) reconstruction by the method in Ref. [20]; (d) the proposed approach after the 100th iteration.

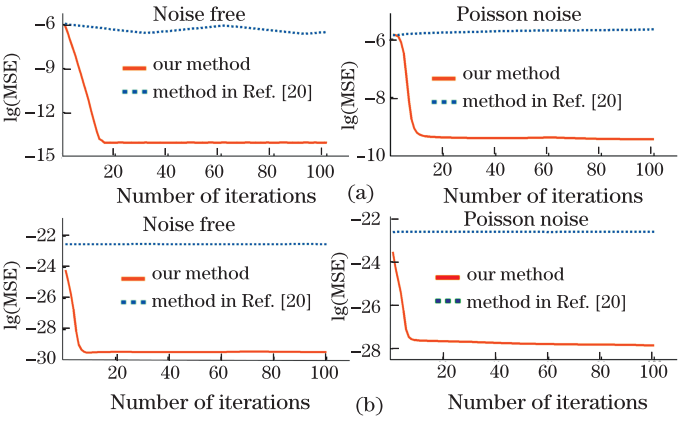

Fig. 3. Comparsion of convergence rates of (a) amplitude and (b) height reconstruction of the 2D complex-valued simulated object.

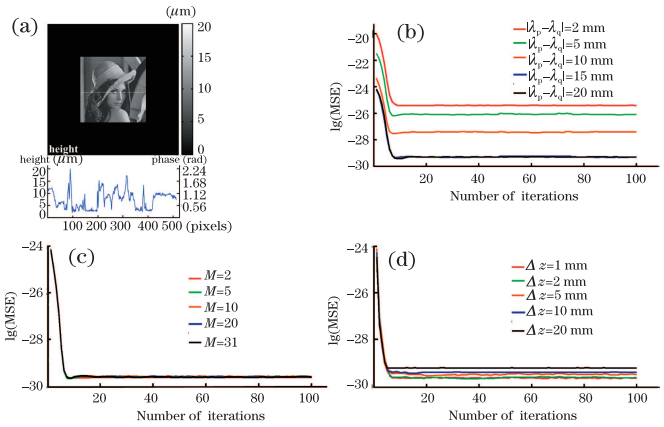

Fig. 4. (a) Test object used for the simulations, of which the gray level indicates the height distributions (0–20 μm); convergence performances under different conditions: (b) different wavelength intervals $|\lambda_p - \lambda_q| = 2$, 5, 10, 15 and 20 nm; (c) different numbers of holograms $M = 2$, 5, 10, 20, and 31; (d) different distance intervals $\Delta z = 1$, 2, 5, 10, and 20 mm.

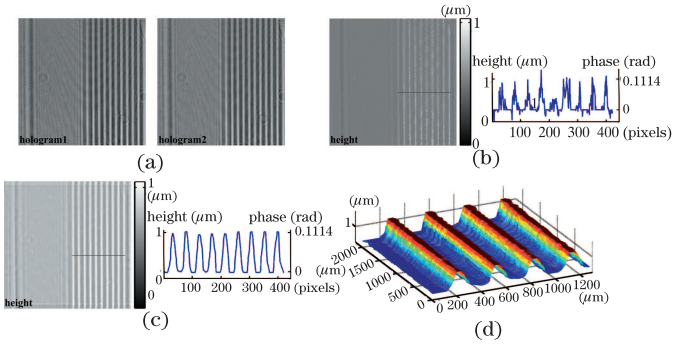

Fig. 5. Experimental result of binary phase grating. (a) Normalized holograms recorded with wavelength of 643.0 and 658.0 nm respectively; (b) reconstruction by the method in Ref. [20]; (c) retrieved distribution by the proposed approach after the 100th iteration; (d) 3D perspective profile of the selected region indicated in (c).

5(d) depicts the three-dimensional (3D) perspective profile for the cutout region indicated in Fig. 5(c). Both the line scan and 3D profile clearly show the peak and valley of the diffraction grating. The depth and period revealed from the reconstructed images match well with the grating's characters. The proposed method shows its applicability for quantiative height measurement.

In conclusion, we present a phase retrieval method to eliminate the twin image for in-line holography from double axially displaced holograms at both dual wavelengths of 643 and 658 nm. By imposing constraints both on the recording planes and object plane, the correct complex field distribution is iteratively retrieved. Based on the concept of the synthetic wavelength, the measurement range of the wrap-free phase is extended to 28.2 μm. By comparing with the iterative approach without any constraint on the object plane[20], the proposed method shows a faster rate of convergence and better elimination of the twin image with less numbers of wavelengths. Since no reference beam or additional moving parts is needed in this technique, it highly immunes to noise or environmental disturbance and provides an alternative tool in profile measurement. Although only weak phase shifting objects are dimonstrated in the experiment, the simulations suggest that the method can be used for objects with larger phase shifts. Like all previous proposed methods, the dispersion effect is neglected in our model, which will be an interesting topic to be investigated in the future.

This work was supported by the National Natural Science Foundation of China (Nos. 31000387, 61177006, and 61307010), China Postdoctoral Research Foundation (No. 2013M540828), and Beijing Postdoctoral Research Foundation (No. 2013ZZ-17).

References

1. D. Gabor, Nature **161,** 777 (1948).
2. K. Nugent, Opt. Commun. **78,** 293 (1990).
3. Y. Ren, C. Chen, R. Chen, G. Zhou, Y. Wang, and T. Xiao, Opt. Express **19,** 4170 (2011).
4. H. Liu, Y. Ren, H. Guo, Y. Xue, H. Xie, T. Xiao, and X. Wu, Chin. Opt. Lett. **10,** 121101 (2012).
5. T. Lei, L. Nick, José A. Domínguez-Caballero, and G. Barbastathis, Appl. Opt. **49,** 1549 (2010).
6. S. Tong, H. Li, and H. Huang, Phys. Rev. Lett. **67,** 3102 (1991).
7. J. Barton, Phys. Rev. Lett. **67,** 3106 (1991).
8. T. Xiao, H. Xu, Y. Zhang, J. Chen, and Z. Xu, J. Mod. Opt. **45,** 343 (1998).
9. Y. Zhang, G. Pedrini, W. Osten, and H. J. Tiziani, Opt. Lett. **29,** 1787 (2004).
10. M. H. Maleki and A. J. Devaney, Opt. Eng. **33,** 3243 (1994).
11. G. Pedrini, W. Osten, and Y. Zhang, Opt. Lett. **30,** 833 (2005).
12. Y. Zhang, G. Pedrini, W. Osten, and H. J. Tiziani, Opt. Express **11,** 3234 (2003).
13. E. J. Candès, T. Strohmer, and V. Voroninski, ArXiv **1,** 1109.4499 (2011).
14. G. Liu and P. D. Scott, J. Opt. Sco. Am. A **4,** 159 (1987).
15. T. Latychevskaia and H. W. Fink, Phys. Rev. Lett. **98,** 233901 (2007).
16. T. Latychevskaia and H. W. Fink, Opt. Express **17,** 10697 (2009).
17. L. Rong, F. Pan, W. Xiao, Y. Li, and F. Wang, Chin. Opt. Lett. **10,** 060902 (2012).
18. J. Gass, A. Dakoff, and M. Kim, Opt. Lett. **28,** 1141 (2003).
19. P. Bao, F. Zhang, G. Pedrini, and W. Osten, Opt. Lett. **33,** 309 (2008).
20. P. Bao,G. Pedrini, and W. Osten, Opt. Commun. **285,** 5029 (2012).
21. W. Goodman, *Introduction to Fourier Optics* (Los Altos, California, 2006).
22. F. Charrière, B. Rappaz, J. Kühn, T. Colomb, P. Marquet, and C. Depeursinge, Opt. Express **15,** 8818 (2007).
23. J. W. Goodman, *Speckle Phenomena in Optics: Theory and Applications* (Roberts and Co., Englewood, 2006).
24. C. Guo, Q. Yue, G. Wei, and L. Lu, Opt. Lett. **33,** 1945 (2008).